ULTRASONIC STIRRING AS A PRODUCTION PROCESS FOR NANOPARTICLE REINFORCED MAGNESIUM ALLOYS AND THE COMPRESSION CREEP RESPONSE OF ZE10 REINFORCED WITH CERIA NANOPARTICLES

H. Dieringa*, N. Hort, K.U. Kainer

Helmholtz-Centre Geesthacht, MagIC – Magnesium Innovation Centre, Max-Planck-Str. 1, 21502 Geesthacht, Germany

**hajo.dieringa@hzg.de*

Keywords: ZE10, nanoparticles, ceria, creep

Abstract

Magnesium alloys reinforced with ceramic particles at micro-scale sizes have increased hardness and wear resistance. However, to improve their high-temperature strength and creep resistance the particles have to be smaller. The optimum size of particles for Orowan strengthening is a diameter less than 100 nm. With a large surface area compared to their weight, any deagglomeration of the nanoparticles in a magnesium melt is difficult to achieve and so requires additional processing. This study uses power ultrasound to break down the agglomeration and finely disperse the ceria nanoparticles. The materials were cast in a permanent mold, direct chill casting process using ceria nanoparticles with a diameter of 40 nm and ZE10 magnesium alloy. Three materials are compared: pure ZE10, cast with and without power ultrasound, and ZE10 reinforced with 1 vol.-% ceria dispersed with ultrasound. Metallography, hardness tests and density measurements were performed. Compression creep tests at 200°C and constant stresses were also performed and the minimum creep rates determined. Moreover, the stress exponent was calculated and the concept of a threshold stress applied.

1 Introduction

Magnesium based composites provide excellent mechanical and physical properties, which are usually an obvious enhancement compared to magnesium matrix alloys. For example, magnesium reinforced with short fibers gave an improvement to the creep resistance of two orders of magnitude in minimum creep rate with Saffil short fiber reinforcement [1]. The strength at high temperatures is often decreased with the introduction of short fibers, and ductility is lost. There appear to be differences between studies of nanoparticle reinforcement of magnesium alloys. For example, SiC-nanoparticle reinforced AS41 alloy showed a 30% increase in yield strength together with a small improvement in ductility [2]. 1.1 % of alumina nanoparticles nearly doubled the yield strength of pure magnesium and even improved ductility from 7.4% to 14% [3]. A similar improvement was found in AZ31 reinforced with alumina [4]. The various nanoparticle reinforced magnesium alloys are summarized in [5]. The excellent properties of all these materials are shadowed by their costly and ineffective

options for production. They are processed by powder metallurgy, which is not useful for the manufacture of gearbox and engine housings, for example. One of the problems that occur in casting processes is to distribute the nanoparticles. Since their surface area is very large compared to their volume they tend to clump and it is difficult to deagglomerate the particles in the metallic melt. Further, the combination of alloy and ceramic reinforcement influences the wettability of the particles. It is not normally possible to distribute ceramic nanoparticles by stirring alone. Added energy is needed to deagglomerate the particles and ultrasound would appear useful for this. This measure is suitable for a permanent mold, direct chill casting process, which was specifically developed for light alloys. The process results in very dense casting without porosity. In this study, magnesium alloy ZE10 with a nominal composition of Mg-1Zn-0.7RE (RE = rare earth elements) is combined with 1 wt.-% ceria nanoparticles. For comparison, the ZE10 was cast with and without ultrasound treatment as well as with ceria added under ultrasound.

2 Materials and testing methods

Commercial ZE10 alloy with a nominal composition of Mg-1Zn-0.7RE (RE=rare earth elements) was cast using a permanent mold, direct chill casting process. After melting the alloy and keeping it at 720°C, the melt was poured into cylindrical molds, which were placed into a round three-zone resistance furnace. A constant flux of Ar-SF6 (5:1) cover gas was introduced on top of the melt during the complete casting and ultrasound process and the melt was superheated to 720°C. The temperature was monitored by a thermocouple in a closed steel tube dipped into the melt. Up to this point, all three materials were processed the same way.

The untreated ZE10 in a steel mold was lowered into a water bath located beneath the ring furnace. Since the mold descended at a constant speed into the water bath, the solidification started at the bottom of the mold. This process is described in [6] and it results in a very dense casting, because the remaining melt is always above the solidified material, which leads to shrinkage feeding at every point. Identical processing steps were performed after an ultrasonic treatment of the pure ZE10 alloy as well as after the adding of 1 wt.-% of ceria (Ce_2O_3) nanoparticles (diameter 40 nm) combined with the ultrasonic treatment. The ultrasound equipment used is shown in Figure 1. It consists of an ultrasound generator UIP1500hd made by the Hielscher company with a frequency of 20 kHz and a maximum power of 1.5 kW. The sonotrode is made of titanium. An ultrasonic treatment was performed for 5 minutes after dipping the sonotrode 15 mm into the melt. For investigations into the microstructure, all materials were ground, polished and etched with picric acid. Optical microscopy was performed with a LEICA DMI5000 M microscope. Density was measured with an accurate weighing machine using the Archimedean principle. Hardness was tested using a Vickers testing facility under a load of 5 kiloponds.

Cylinders with a diameter of 6 mm and a length of 15 mm were prepared using the spark erosion technique for compression tests. The creep tests were performed by ATS Lever Arm Test Systems under constant stresses of 80, 100 and 120 MPa and a temperature of 175°C.

Figure 1. Ultrasound generator (left) with attached booster and sonotrode

3 Results and Discussion

3.1 Microstructure and Density

The casting process using a permanent mold, direct chill process was successfully performed and the castings were free of pores. This was verified by density measurements performed on all materials. The density was determined according to the Archimedean principle and both ZE10 alloys (with and without ultrasonic treatment) gave the same value of 1.7682 g/cm^3. Unexpectedly, the ceria-reinforced composite had a slightly lower density of 1.7530 g/cm^3. Since ceria has a density of 6.2 g/cm^3, the resulting density of the composite, according to the rule of mixtures, should have been 1.8125 g/cm^3. One explanation for this could be reaction products at the interface between the matrix and nanoparticle, with a high volume or particle agglomerations with gas inclusions.

Figure 2 shows micrographs of all three materials, i.e. ZE10 (a), ZE10 with ultrasound (US) (b) and ZE10 with the addition of 1 wt.-% ceria introduced under ultrasonic treatment (c). The grain size in the untreated ZE10 is 74 µm and under ultrasound there is a slight refinement to 69 µm. A grain refinement under ultrasonic treatment has been observed elsewhere [7, 8]. With the addition of ceria nanoparticles under ultrasound, the grain size is larger at 89 µm. This was also unexpected, because the dispersed nanoparticles were foreseen as acting as nuclei for solidification and thus contributing to further grain refinement.

Not only the grain size, but also the shape of the grains differed. The nanoparticle reinforced material has a globular shaped grain structure; whereas the ultrasound treated ZE10 has a dendritic solidification microstructure. By contrast, the untreated ZE10 has both dendritic and globular grains. The hardness determined is nearly identical for all three materials in the range of 39 HV5. The microstructural features and the densities measured are set out in Table 1.

	ZE10	ZE10 + US	ZE10 + US + ceria
Grain size [µm]	74	69	89
Vickers hardness [HV5]	39.7±1.8	38.5±1.7	38.3±2.9
Density [g/cm^3]	1.7682	1.7682	1.7530

Table 1. Grain size, hardness and density of the three ZE10 based materials.

3.2 Creep

Metal tends to creep slowly under elevated temperatures and stresses. Quite often creep tests are measured under tensile stress. This is the case for materials tested under rotation, for turbine blades for instance. In contrast to high-strength metals, lightweight alloys are usually tested for applications of creep under compressive stress, for example bolted in gearbox housings and crankcases. The high temperatures result from the engine's heat and the stress from the bolting. In addition, bolts with lower coefficient of thermal expansion (CTE) compared to the case alloy can even deteriorate the creep deformation, because when heated up, the lower deforming bolt improves the stress applied to the housing. After cooling, this effect can lead to a catastrophic leakage and loss of oil.

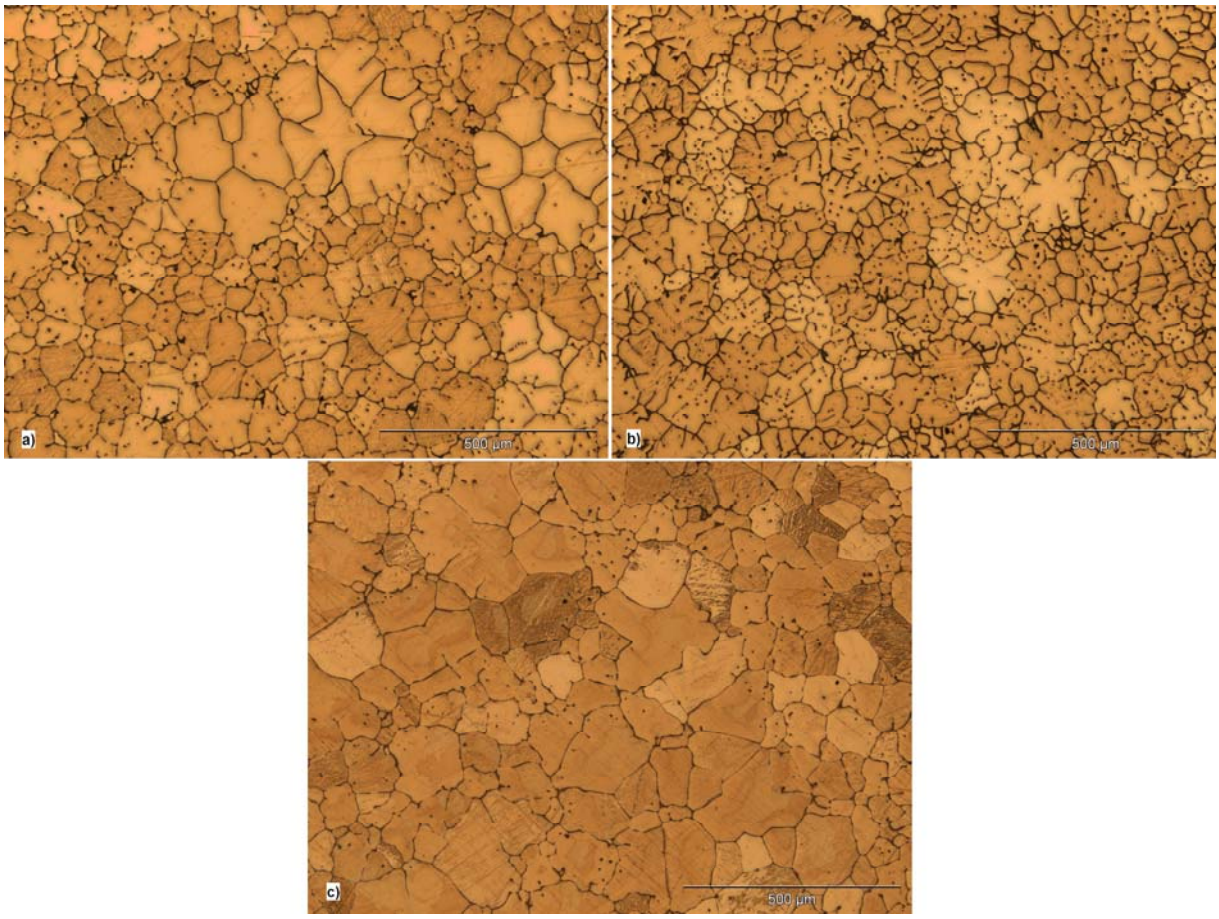

Figure 2. Microstructure of (a) ZE10 cast without additional treatment, (b) ZE10 with ultrasonic treatment, and (c) with reinforcement of 1 wt.-% ceria added under ultrasound.

Temperature (T) and stress (σ) dependence of minimum creep rate $\dot{\varepsilon}_s$ (=$d\varepsilon_s/dt$) is usually given in the Norton-Equation (1):

$$\dot{\varepsilon}_s = \frac{ADGb}{kT}\left(\frac{\sigma}{G}\right)^n \tag{1}$$

Where A is a dimensionless constant that depends on the material, D the diffusion coefficient (=$D_0 \exp(-Q_c/RT)$ where D_0 is the frequency factor, Q_c the activation energy for creep, R the gas constant, and T the absolute temperature), G is the shear modulus, b the Burgers vector and k the Boltzmann constant.

Creep curves of compression creep tests at 200°C and 80 MPa of all three materials are shown in Figure 3a. After a primary stage when the materials strain-harden, a secondary creep stage with an almost constant creep rate follows. Figure 3b shows the creep rate as a function of time. The highest minimum creep rate is found for the ZE10, the lowest for the ZE10+US+ceria and between these the ultrasonic treated ZE10. It is not only the minimum creep rate that contributes to making a creep-resistant material identifiable. The extent of deformation after a certain time is also connected to the primary deformation. It is clear to see

in Figure 3a that at every point the amount of deformation is lowest in the ceria reinforced and ultrasound-treated ZE10. It is less than half the deformation of the untreated ZE10 and deformation of the ultrasonic treated ZE10 without ceria nanoparticles lies between.

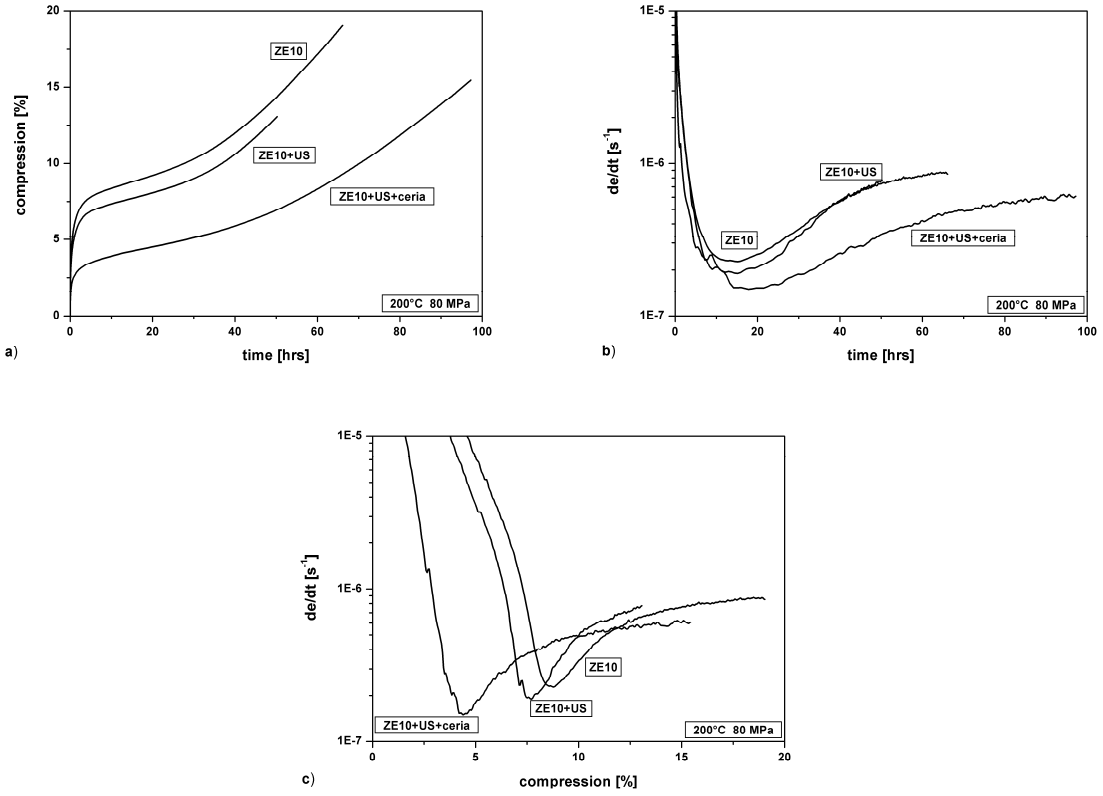

Figure 3. Creep curves from tests performed at 200°C and 80 MPa. (a) Deformation over time, (b) deformation rate over time and (c) deformation rate over deformation.

After performing several creep tests at one temperature and different applied stresses, it is possible to determine the stress exponent n from double-logarithmic plots of minimum creep rates from the tests as a function of applied stress. In accordance with (1), the slope of the fitted line is n. These plots can be seen in Figure 4a. The stress exponents determined are given in Table 2.

It is an accepted fact that the stress exponent and the activation energy for creep can provide information about the deformation mechanisms that control the rate during creep. From a physical point of view, it is necessary for creep deformation to occur at every stress applied. However, in reality this is not the case for all materials. Precipitation or particle strengthened alloys deform only above a certain stress, why this is referred to as the threshold stress σ_0. The threshold stress reduces the applied stress σ in a way that the achieved true stress σ_t is more suitable as the stress for calculating the stress exponent and is why this is called the true stress exponent n_t.

$$\sigma - \sigma_0 = \sigma_t \tag{2}$$

From (2) follows (3).

$$\dot{\varepsilon}_s = \frac{ADGb}{kT}\left(\frac{\sigma-\sigma_0}{G}\right)^{n_t} \quad (3)$$

High stress exponents are often identified in creep tests with dispersion strengthened materials or metal matrix composites. These are explained by the appearance of a threshold stress σ_0, which reduces the applied stress σ and is connected to phenomena of interaction between particle obstacles and dislocations. Three explanations can be found in metallic materials:

- Threshold stress is the stress that is needed to bend a dislocation between two obstacles [9-11], corresponding to the Orowan stress.
- Threshold stress corresponds to an additional back stress, which is built up while climbing over an obstacle, and is needed to elongate the dislocation [12].
- Threshold stress corresponds to an additional stress, which is needed after climbing over an obstacle, to detach from it [13, 14].

The stress exponent n or the true stress exponent n_t is directly related to deformation mechanisms taking place during creep. A value of n=3 is related to a viscous glide of dislocations [15-17], n=5 is related to dislocation climbing at high temperatures [15, 16, 18] and n = 7 to dislocation climbing at low temperatures [19]. A value of n=1 is connected to diffusion deformation mechanisms [20, 21].

Several procedures have been discussed for evaluating the threshold stress from minimum creep rates, identified at different stresses and one temperature. It is possible to determine the threshold stress by plotting $\dot{\varepsilon}^{1/n}$ against σ on a linear axis and extrapolate to zero strain rates [22]. The disadvantage of this method is the predefinition of n, which is usually chosen as 3, 5 or 7 in cases of dislocation motion as the rate controlling deformation processes. A simpler procedure was developed by Li and Langdon [23]. The threshold stress is defined as the stress below which no creep deformation takes place. A creep rate of $1*10^{-10}$ s^{-1} is the slowest deformation that can be conventionally measured and represents a deformation of 1% over three years.

	ZE10	ZE10 + US	ZE10 + US + ceria
Stress exponent n	9.3	9.0	8.6
Threshold stress σ_0	38.5	40.0	42.8
True stress exponent n_t	5.5	5.2	4.7

Table 2. Stress exponents, threshold stresses and true stress exponents determined from tests at 200°C.

Double logarithmic plots of minimum creep rate versus applied stress extrapolated to $1*10^{-10}$ s^{-1} should therefore give the threshold stress. According to this procedure the threshold stresses were determined as shown in Table 2.

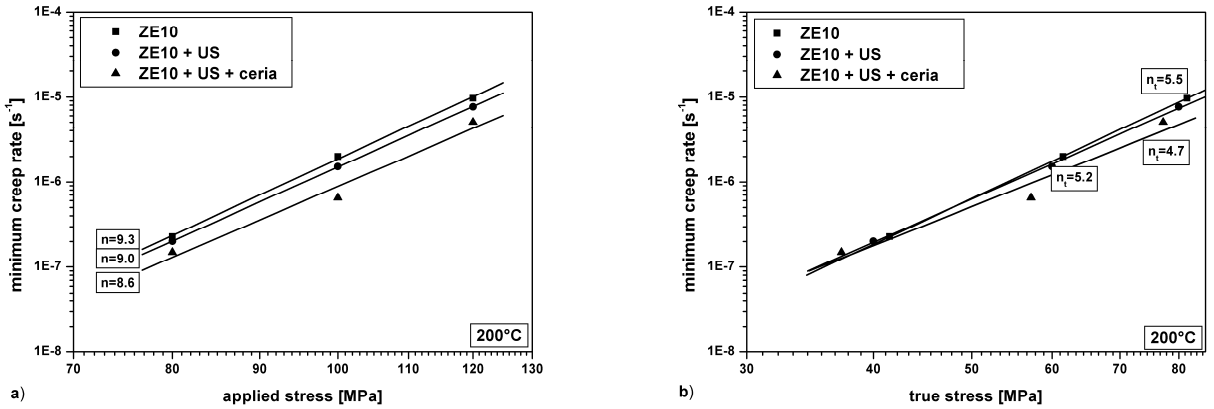

Figure 4. Plots of minimum creep rate over applied stress (a) and true stress (b) from creep tests at 200°C for determination of stress exponents and true stress exponents.

4 Conclusions

In this study, the magnesium alloy ZE10 with and without ultrasonic treatment, and with and without ceria nanoparticles was successfully cast in a permanent mold direct chill casting process. All three materials have comparable hardness and both the pure ZE10 alloys have the same density. The ceria reinforced composite has a slightly lower density and this was unexpected, because the density of ceria is 6.2 g/cm^3. An explanation for its lower density is a possible chemical reaction on the surface of the particles that led to reaction products resulting in a higher volume compared to the ceria and magnesium alone. The grain size of the ultrasonic treated ZE10 is lower compared to the untreated ZE10, which is attributed to the ultrasonic treatment. Previous investigations have encountered similar results. The ceria reinforced ZE10 gives the largest grains. The grain shapes also differ in the materials. The composite has a globular grain structure, whereas the ultrasonic treated ZE10 is dendritic. The untreated ZE10 shares both characteristics. Creep tests at 200°C and stresses of 80, 100 and 120 MPa were performed in compression. Ceria reinforced ZE10 resulted in the best creep resistance, not only in terms of minimum creep rate, but also primary creep deformation. This is followed by the ultrasonic treated ZE10 and then the untreated ZE10. From the minimum creep rates, the true stress exponents were determined according to the concept of threshold stresses. True stress exponents of n_t=5 indicate a dislocation climb is the rate-controlling deformation process during creep.

5 References

[1] Dieringa H., Hort N. Kainer K.U. *Comparison of tensile and compressive creep data of AE42 magnesium alloy and its short fibre reinforced composite*; *Processing and Fabrication of Advanced Materials XVI*; 17.-19.Dec. 2007 in Singapore (2008) ISBN: 978-981-05-9650-7; pp. 248-255.

[2] Cao G, Konishi H, Li X Mechanical properties and microstructure of SiC-reinforced Mg-(2,4)Al-1Si nanocomposites fabricated by ultrasonic cavitation based solidification processing. Mater. Sci. Eng., A486, pp 357-362 (2008).

[3] Hassan S.F., Gupta M. Enhancing Physical and Mechanical Properties of Mg Using Nanosized Al2O3 Particulates as Reinforcement. *Metall. Mater. Trans.* **36A**, pp 2253-2258 (2005).

[4] Paramsothy M., Hassan S.F., Bau N.Q., Srikanth N., Gupta M. Selective Enhancement of Tensile/Compressive Strength and Ductility of AZ31 Magnesium Alloy via nano-AL2O3 Reinforcement Integration Method Alteration. *Mater Sci Forum* **618–619**, pp 423-427 (2009).

[5] Dieringa H. Properties of magnesium alloys reinforced with nanoparticles and carbon nanotubes: a review. *J. Mater. Sci.* **46**, pp 289-306 (2011).
[6] Elsayed F., Hort N., Salgado-Ordorica M., Kainer K.U. Magnesium permanent mold casting optimization. *Mat. Sci. Forum* **690**, pp 65-68 (2011).
[7] Khosro Aghayani M., Niroumand B. Effects of ultrasonic treatment on microstructure and tensile strength of AZ91 magnesium alloy. *J. Alloys Compounds* **509**, pp 114-122 (2011).
[8] Eskin G.I. Crystallization of ingots of magnesium alloys with ultrasonic treatment of the melt. *Metallurgist* **47**, 7-8, pp 265-272 (2003).
[9] Olliver W.C., Nix W.D. High temperature deformation of oxide dispersion strengthened Al and Al-Mg solid solutions. *Acta Metall.* **30**, pp 1335-1339 1982.
[10] Orowan E. in: Cohen M. (Ed.) Dislocation in Metals, *AIME*, New York p 131 (1954).
[11] Kocks U.F. A statistical theory of flow stress and work-hardening; *Phil. Mag.* **13**, pp 541-566 (1966).
[12] Arzt E., Ashby M.F. Threshold stresses in Materials containing dispersed particles. *Scr. Metall.* **16**, pp 1285-1290 (1982).
[13] Arzt E., Wilkinson D.S. Threshold stresses for dislocation climb over hard particles: the effect of an attractive interaction. *Acta Metall.* **34**, pp 1893-1898 (1986).
[14] Arzt E., Rösler J.: The kinetics of dislocation climb over hard particles: effects of an attractive particle-dislocation interaction; *Acta Metall.* **36**, pp 1053-1060 (1988).
[15] Sherby O.D., Burke P.M. Mechanical behavior of crystalline solids at elevated temperature. *Progress in Mater. Sc.* **13**, pp 325-389 (1968).
[16] Mohamed F.A., Park K.T., Lavernia E.J. Creep behavior of discontinuous SiC-Al composites. *Mat. Sc. Engin.* **A150**, pp 21-35 (1992).
[17] Weertman J. Steady-state creep through dislocation climb. *J. Appl. Phys.* **28**, 3 pp 362-364 (1957).
[18] Weertman J. Steady-State Creep of Crystals. *J. Appl. Phys.* **28**, 4 pp 1185-1189 (1957).
[19] Robinson S.L., Sherby O.D. Mechanical behavior of polycrystalline tungsten at elevated temperature. *Acta Met.* **17**, pp 109-125 (1969).
[20] Harper J., Dorn J.E. Viscous creep of aluminum near its melting temperature. *Acta Met.* **5**, pp 654-665 (1957).
[21] Ardell A.J., Lee S.S. A dislocation network theory of Harper-Dorn creep - I. Steady state creep of monocrystalline Al. *Acta Met.* **34**, pp 2411-2423 (1986).
[22] Lagneborg R., Bergman B. The stress/creep rate behaviour of precipitation-hardened alloys. *Metal Sci.* **10**, pp 20-28 (1976).
[23] Li Y., Langdon T.G. A simple procedure for estimating threshold stresses in the creep of metal matrix compopsites. *Scripta Mat.* **36**, 12, pp 1457-1460 (1997).